Detecting beta-amyloid glycation by intrinsic fluorescence - understanding the link between diabetes and Alzheimer's disease.

Abeer Alghamdi[a], Shareen Forbes[b], David J.S. Birch[a], Vladislav Vyshemirsky[c] and Olaf J. Rolinski*[a]

[a]Department of Physics, University of Strathclyde, Glasgow G4 0NG, UK.
[b] BHF Centre for Cardiovascular Science, The Queen's Medical Research Institute, University of Edinburgh, Edinburgh EH16 4TJ, UK.
[c]School of Mathematics and Statistics, University of Glasgow, Glasgow G12 8QQ, UK.

Abstract

We monitor early stages of beta-amyloid ($A\beta_{1-40}$) aggregation, one of key processes leading to Alzheimer's disease (AD), in the presence of high glucose concentrations by measuring $A\beta_{1-40}$ intrinsic fluorescence. The multiple peaks and their shifts observed in the time-resolved emission spectra (TRES) reveal the impact of glycation on $A\beta_{1-40}$ oligomerisation. The results show that formation of the advanced glycation end products (AGEs) alters the aggregation pathway. These changes are highly relevant to our understanding of the pathophysiology of AD and the implication of AGE and diabetes in these pathways.

TOC Graphic:

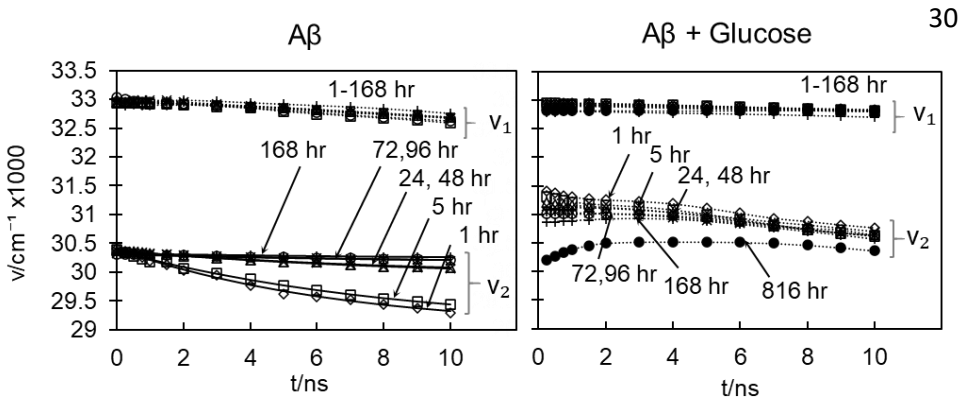

Keywords: Beta-amyloid aggregation, Alzheimer's disease, Tyrosine fluorescence decay, glycation, time-resolved emission spectra.

Introduction

Alzheimer's disease (AD) is the most common cause of dementia. Currently there is no general agreement on what activates the progression of AD, multiple triggering events in the early stages of AD have been suggested. They all appear to converge to a few final pathways in the late stages, which lead to the inflammation and neurodegeneration that characterise the condition. The triggering compounds investigated included metal ions (e.g. Cu, Zn and Fe ions)[1,2] and glycation factors (e.g. glucose[3] and fructose[4]).

In this paper we are mostly concerned with the involvement of advanced glycation end products (AGEs) in AD pathogenesis. AGEs relation with brain aging and AD was first proposed in the mid-1990s[5] . AGEs accumulate in cells and tissues and their accumulation is accelerated in the case of AD. Several studies have demonstrated that patients with diabetes show a greater deposition of AGEs in the brain and receptors for AGEs (RAGE)[5,6]. Therefore, it is widely accepted that AGEs are active participants in the progression of AD[7–10]. More importantly, recent studies have demonstrated that glycated beta-amyloids (Aβ), a naturally occurring peptide capable of binding to sugars and resulting in the formation of AGEs, are more toxic than non-glycated Aβ amyloids[11,12], i.e. it was found that Aβ-AGE were more active than Aβ in decreasing cell viability (e.g. 8-DIV embryonic hippocampal neurons), increasing cell apoptosis, inducing tau hyperphosphorylation, and reducing synaptic proteins[11]. In vivo studies performed on rats[12] show that Aβ-AGE exacerbates Aβ-mediated cognitive impairment and neuropathology.

Detecting the aggregation of glycated and non-glycated Aβ amyloids can be challenging particularly at the early stages of this process. Most techniques that have been used to study Aβ glycation such as atomic force microscopy (AFM)[13–15], electron microscopy[16], dynamic light scattering (DLS)[15], circular dichroism (CD)[11,15] and Thioflavin T (ThT)-based fluorometry[17] are evidently sensitive to fibril formation (i.e. the formation of Aβ beta-sheets). However, they lack the specificity to detect Aβ oligomerization. This drawback hinders the progress in understanding of what triggers the progression of AD and how the symptoms associated with the disease can be prevented.

The accepted model describing the aggregation of the most abundant form $A\beta_{1-40}$ is the nucleation-dependent polymerization model, which is characterized by two distinct stages: a lag phase, followed by a rapid elongation phase. It is believed, that the initial monomers gradually form dimers, trimers and larger oligomers (a lag phase), and, at later stages, beta-sheets, protofibrils and fibrils. Conventional methods typically used to study this reaction (i.e. ThT-based fluorimetry) are reporting fibril formation but are not sensitive to events taking place early in the lag phase, promoting the assumption that only Aβ monomers and large oligomers exist at early stages and that the lag time is defined by the primary

nucleation rate only. However, the existence of oligomer intermediates prior to fibril formation has been confirmed by AFM, electron microscopy and dynamic DLS [3,5,10,12,15,18–20]. Although the oligomers are considered to be more toxic than mature insoluble fibrils[20,21],there are only few attempts to quantify the extent of oligomer formation, determine whether they are kinetically competent to form amyloid fibrils or to identify the mechanism by which oligomers trigger neurodegeneration. Here we attempt to address these tasks by using sensing potential of the intrinsic Tyrosine fluorescence.

Most researchers track amyloid-β aggregation reactions using extrinsic fluorophores mostly because such a fluorescence capability is available in most laboratories. ThT fluorescence is commonly used to detect Aβ aggregation even though it cannot detect early oligomer formation[22–24]. Recent reports suggest the usefulness of the fluorophore 1,1'-bis(anilino)-4-,4'-bis(naphthalene)-8,8'-disulfonate (bis-ANS) for the detection of Aβ aggregation, however, there is no agreement on whether bis-ANS binds most strongly with oligomers[25] or fibrils[26]. Another disadvantage of using extrinsic fluorophores in amyloid aggregation studies is the fact that the ratio of fluorophore to Aβ can significantly influence the obtained results[26]. Moreover, it has been reported that some extrinsic fluorophores such as bis-ANS[26] and ThT[27] might affect the nucleation rate in some cases, or even prevent aggregation[28].

To avoid these complications, we have adopted an approach that exploits the intrinsic fluorescence of Aβ. The peptide $A\beta_{1\text{-}40}$ contains a single tyrosine residue (Tyr_{10}) in addition to two phenylalanine residues (Phe_{19}, Phe_{20}). Upon excitation at 280 nm, the intrinsic fluorescence of the peptide represents the fluorescence of the sole tyrosine residue. Time resolved spectroscopy studies of Tyr in $A\beta_{1\text{-}40}$ show that its fluorescence intensity decay at detection wavelength 315 nm is sensitive to peptide aggregation especially at its earliest stage[22,29,30]. To better understand the underlying kinetics of this complicated molecular system, we have measured a collection of a series of decay curves across the Tyr spectrum[31] for the purpose of constructing the time resolved emission spectra (TRES). The analysis of TRES has demonstrated that dielectric relaxation affects substantially the fluorescence decays of Tyr in Aβ, which helped to better understand the evolution of underlying fluorescence kinetics, thus better explaining the development of oligomerisation.

Note that we investigate the fluorescence of Tyr in $A\beta_{1\text{-}40}$ in the presence of high glucose concentrations. Our objective was to investigate fluorescence changes caused by both peptide glycation and aggregation to reveal the impact of glycation on $A\beta_{1\text{-}40}$ oligomerisation. In order to cause aggregation and glycation occurring in the similar time scales, we have chosen higher than physiological concentration of glucose (50 mM).

Results and discussion

Steady-state fluorescence spectra were obtained for $A\beta_{1-40}$ with and without high glucose (Fig. 1). The samples were measured using different excitation wavelengths and at different stages of aggregation. The spectra observed at excitation 279 nm (Fig.1a) for both samples is the typical spectrum of Tyr. As the samples age, the fluorescence intensity decreases and the spectrum of the sample with glucose exhibits a considerable change in its shape.

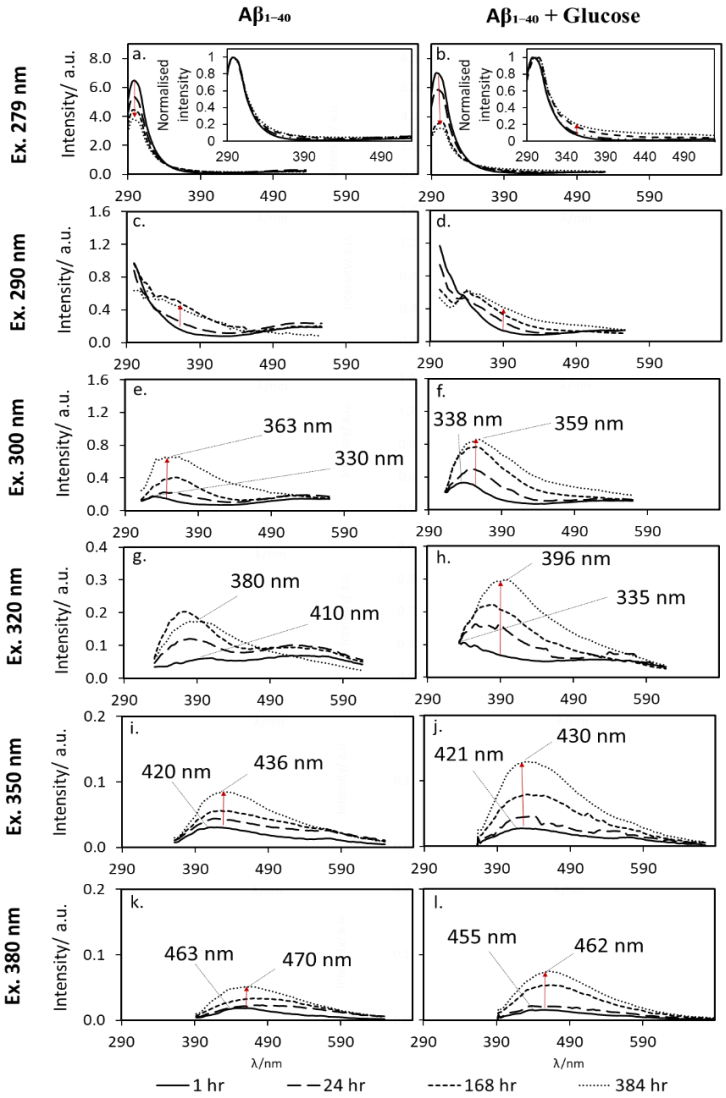

Figure 1:Fluorescence spectrum of 50 µM $A\beta_{1-40}$ in PBS buffer (10 mM, pH 7.4) measured in the absence (left) and presence (right) of 50 mM glucose at excitation wavelengths 279 nm (a, b), 290 nm (c, d), 300 nm (e, f), 320 nm (g, h), 350 nm (i, j) and 380 nm (k, l) and after incubation for 1 hr (solid), 24 hr (long-dash), 168 hr (short-dash) and 384 hr (dotted). The arrow shows direction of the flow of time (measurements taken at 1 hr, 24hrs, 168 hrs and 386 hrs after sample preparation). Normalised emission spectra of both samples at excitation wavelength 279 nm are shown in a and b insets.

Although Tyr doesn't absorb light at wavelengths above 300 nm, when Tyr in $A\beta_{1-40}$ is excited at wavelengths ≥ 300 nm fluorescence peaks are observed at higher wavelengths. Fig. 2 shows the emission of $A\beta_{1-40}$ in the absence and presence of glucose. In general, the emission is time and excitation-wavelength dependent. At the excitation wavelengths ≥ 300 nm the position of the emission peak increases with the excitation wavelength and the spectrum peak position moves towards red with time. These observations suggest that Aβ's monomers aggregate and form at least one fluorescent complex within few hours and a variety of complexes of the broad distribution of sizes, as evidenced by the excitation wavelength - emission peaks correlation, within few days. The spectroscopic origin for the spectral shift is not known.

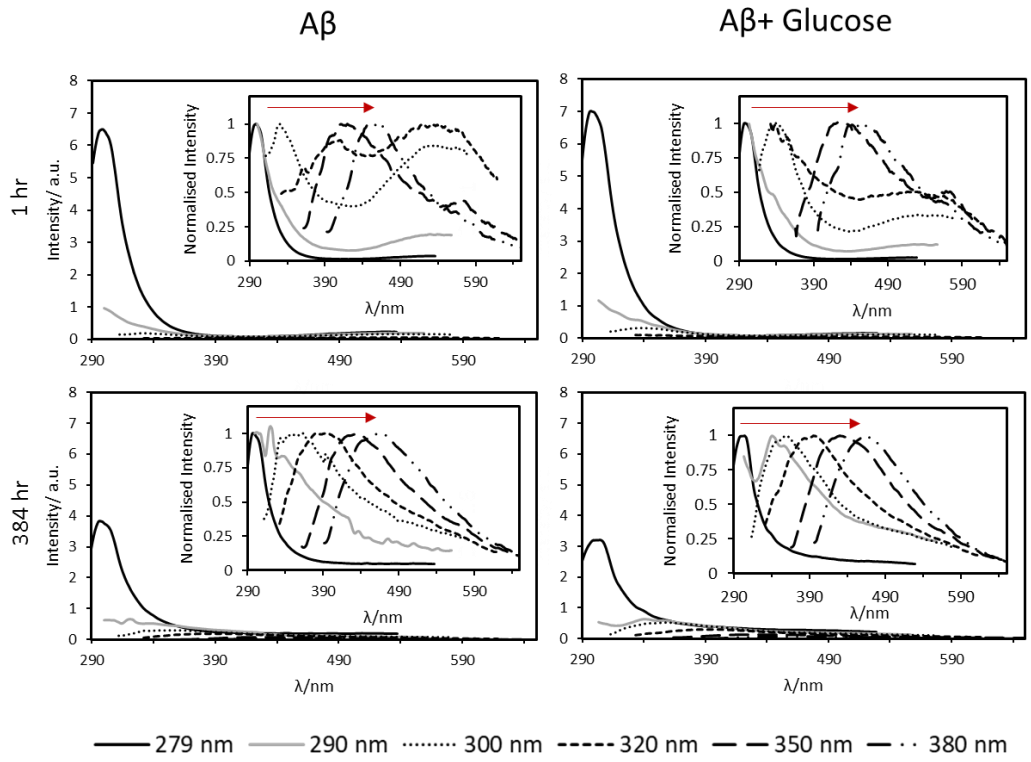

Figure 2. Steady-state measurements of 50 μM $A\beta_{1-40}$ in PBS buffer (10 mM, pH 7.4) in the absence (left) and presence (right) of 50 mM glucose at excitation wavelengths 279 nm (solid black), 290 nm (solid grey), 300 nm (dotted), 320 nm (short-dash), 350 nm (long-dash) and 380 nm (dash-dot-dot) after incubation for 1 hr (top) and 384 hr (bottom). Insets show the normalised emission spectra.

TRES measurements were performed for $A\beta_{1-40}$ (50 μM) at several stages of aggregation, namely 1, 5, 24, 48, 72, 96 and 168 hrs after sample preparation (the number indicates the age of the sample when each series of measurements is started). Fig. 3 shows an example of TRES at two stages of aggregation: 1 and 168 hours from sample preparation in the absence and presence of glucose (50 mM). Experimental data were fitted to a model based on the Toptygin and Brand[32] approach, which assumes that the fluorescence spectrum $I_t(\nu)$ of a single fluorescent residue can be expressed as $\sim\nu^3 g(\nu)$, where $g(\nu)$ is

the Gaussian distribution function. Consequently, the spectrum of a sample with *N* fluorescent residues would be described by the sum of *N* normalized functions of the type $\sim \nu^3 g(\nu)$.

$$I_t(\nu) = \sum_{i=1}^{N} \frac{C_i(t)\nu^3 exp\left[-\left(\nu-\nu_i(t)\right)^2/(2\sigma_i^2(t))\right]}{\sqrt{2\pi}\,\nu_i(t)\,\sigma_i(t)\,(\nu_i{}^2(t)+3\sigma_i^2(t))} \qquad (1)$$

where *t* is the time after excitation in ns, ν is wavenumber in cm^{-1}, $\sigma_i(t)$ is the standard deviation of each component, $\nu_i(t)$ is its peak position and $C_i(t)$ - the fluorescence intensity contribution of the *i*-th component at the time *t*, i.e. the fluorescence intensity decay of this component.

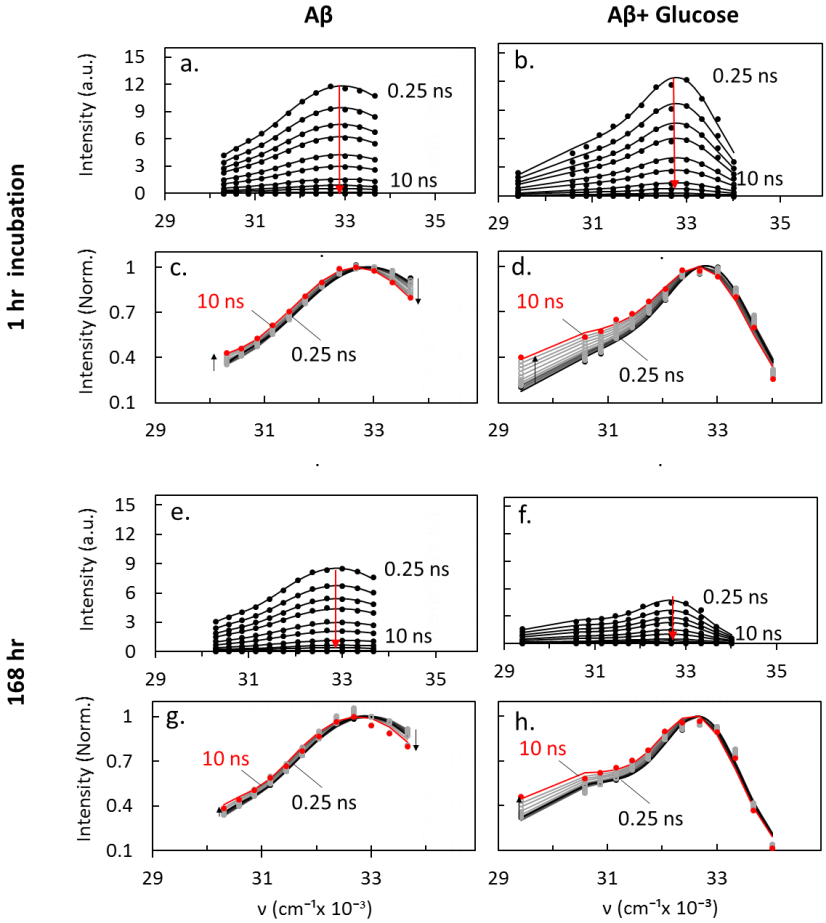

Figure 3 : Time-resolved emission spectra (TRES) obtained for 50 µM $A\beta_{1-40}$ in HEPES buffer (0.1 µM, pH 7.4) after 1hr of incubation (a) and 168 hr of incubation (e). TRES obtained for 50 µM $A\beta_{1-40}$ in the presence of 50mM glucose after 1 hr of incubation (b) and 168 hr of incubation (f). Normalised TRES for $A\beta_{1-40}$ in the absence and presence of glucose after 1hr of incubation (c,d) and 168 hr of incubation (g,h) The solid lines represent the two-Toptygin type functions fits.

In our previous work[31] we have demonstrated that the spectra of free $A\beta_{1-40}$ can be sufficiently described by two peaks. The presence of non-aggregating monomers and aggregating oligomers in the sample explains this double-peak structure of the spectra. Note that we only study the fluorescence decays of the Tyr residues excited at 279 nm, not the fluorescent products of oligomerisation, which require longer excitation wavelengths and their fluorescence intensities are too low for detecting fluorescence intensity decays using traditional time-correlated single photon counting (TCSPC) instrumentation. The red

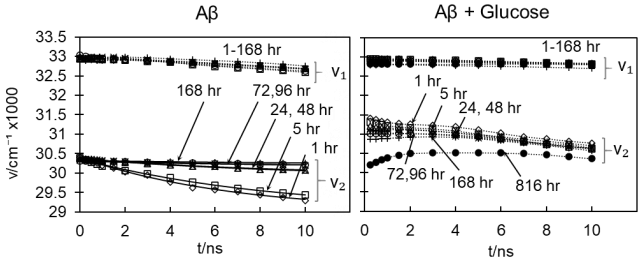

Figure 4: Peaks position ν1 (t) and ν2 (t), obtained from fitting $A\beta_{1-40}$ TRES to equation (1), plotted against time in nanoseconds at different stages of aggregation (1 hr, 5 hr, 24 hr, 48 hr, 72 hr, 96 hr and 168 hr) for sample with and without glucose.

shifts observed for each peak individually[31] represent two different rates of dielectric relaxation. The TRES of $A\beta_{1-40}$ with glucose also demonstrated the presence of two components (N=2). For the purpose of understanding the underlying fluorescence kinetics of $A\beta_{1-40}$ in the presence of 50 mM of glucose, we compared the parameters obtained from fitting the model TRES (equation (1) for N=2) to the experimental data of $A\beta_{1-40}$ with glucose with those recovered from the sample without glucose.

Fig. 4 illustrates the position of the two peaks $v_1(t)$ and $v_2(t)$, recovered from fitting equation (1) to experimental TRES, in the presence and absence of glucose. Position of the first peak $v_1(t)$ for samples with and without glucose is located at ~33000 cm^{-1} at $t=0$. $v_1(t)$ in both samples exhibit nearly no changes over 10 ns after excitation, which indicates that dielectric relaxation is very fast, thus nearly completed before fluorescence occurs. The location of the peak in the spectra and the fast dielectric relaxation is consistent with monomers being responsible of this emission. This also demonstrates the characteristic resemblance in the behaviour of this peak in the samples with and without glucose.

The second peak $v_2(t)$ is highly influenced by the presence of glucose as shown in Fig.4. Its position in a no-glucose sample is located at ~30500 cm^{-1} at $t=0$. The changes observed in the position of $v_2(t)$ during 10 ns after excitation varies depending on the age of the sample. When the sample is 1 hr old we observe an exponential shift, caused by dielectric relaxation, from $v_2(0) \approx 30500$ cm^{-1} to $v_2(\infty) \approx 29000$ cm^{-1} with the dielectric relaxation time $\tau_R = 6.7$ ns. As the sample aggregation progresses the relaxation time τ_R increases and the red shift decreases, which can be explained by gradual growth in the size of the aggregates. We attribute this component to oligomers because aggregation explains why the initial

position of the peak $v_2(0)$ appears at a substantially lower energy value (30500 cm^{-1}) and explains the red shift after excitation.

In the presence of glucose, $v_2(t)$ behaves in a different manner (Fig. 4). The initial position of the second peak $v_2(0) \approx 31500$ cm^{-1} for a fresh sample and gradually decreases as the sample ages. The position of the second peak $v_2(t)$ shifts towards lower energies within 10 ns but not exponentially as observed in free $A\beta_{1\text{-}40}$. This might indicate that this peak represents more than one component where each has its own intensity decay and dielectric relaxation rate. The initial position of the peak and its behaviour in the nano-second time scale might be a result of $A\beta_{1\text{-}40}$ binding to glucose and/or alterations in the $A\beta_{1\text{-}40}$ aggregation pathway caused by the presence of glucose.

It is essential to mention, that because we detected the shifts in the transient emission spectra occurring in the same time scale as fluorescence, each of the measured experimental fluorescence intensity decays $I_v(t)$ is a combination of the decay of the population of excited states and the effect of dielectric relaxation.[29] Therefore we fitted multiexponential functions to the experimental decays and used them as mathematical representations of these decays in TRES procedure, but no physical meaning can be attributed to the individual recovered time constants and pre-exponential factors.

Further insights on the development of oligomerisation of both samples can be obtained from the analysis of other parameters extracted from fitting equation (1) to the data. The $C_1(t)$ and $C_2(t)$ functions represent the fluorescence intensity decay of each component individually (Fig. 5a and b). In the free $A\beta_{1\text{-}40}$ sample, $C_1(t)$ decays with a characteristic lifetime T_1 regardless of the samples actual age (Fig. 5d). This corresponds with our previous assumption that the $C_1(t)$ component is mostly monomers. The characteristic lifetime T_2 of the decay $C_2(t)$, however, decreases with aggregation. The initial value of the ratio $C_1(0)/C_2(0)$ indicates the dominance of monomer's emission, which then slightly decreases with time, indicating that aggregates are being formed.

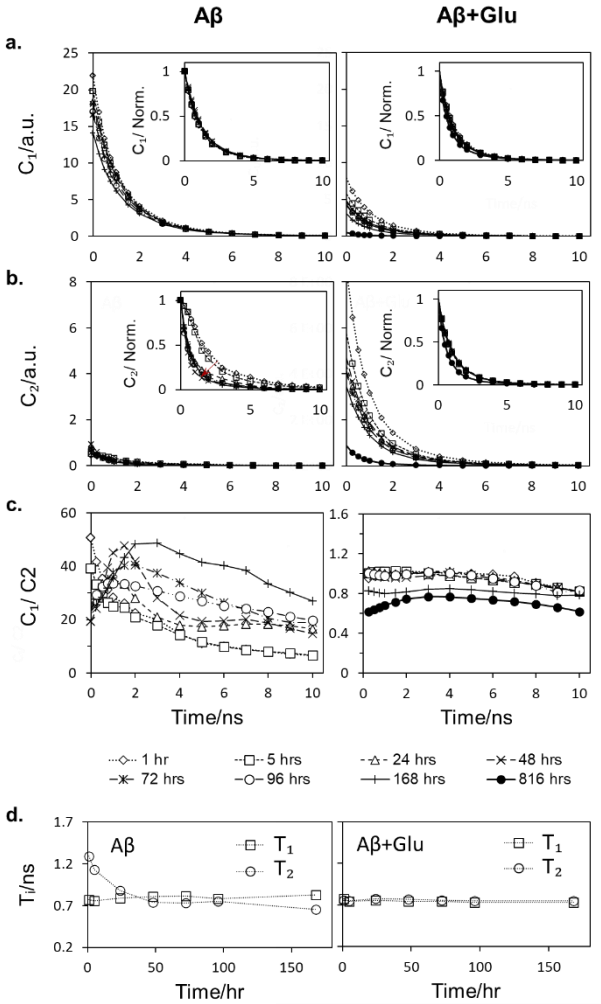

Fig.5 The fluorescence intensity decays of the two emitting specie; monomers $C_1(t)$ (a) and oligomers $C_2(t)$ (b), obtained from fitting TRES to equation (1), and the ratio of monomer to oligomer contribution $C_1(t)/C_2(t)$ (c) in the absence (left) and presence (right) of glucose. The characteristic fluorescence lifetimes of monomers T_1 and oligomers T_2 (d) in the absence (left) and presence (right) of glucose.

The ratio $C_1(0)/C_2(0)$ cannot be associated directly with the concentration of monomers and oligomers in the sample because it is likely that the quantum yield of Tyr in a monomer is reduced to some extent when the monomers aggregate and form oligomers. Nevertheless, the $C_1(t)/C_2(t)$ plot for free $A\beta_{1\text{-}40}$, shown in Fig. 5c, is highly sensitive to the age of the sample and can be used to indicate the stage of $A\beta_{1\text{-}40}$ aggregation.

In the presence of glucose, however, $C_1(t)$ and $C_2(t)$ decay with similar and constant rates at least during the first 168 hrs (Figs. 5a, b and d). However, when the sample is 816 hr old, $C_2(t)$ decays much faster. The ratio $C_1(0)/C_2(0) \approx 1$ indicating that, in the presence of glucose, monomers contribute to only 50% of the emission, which is considerably low compared with the free $A\beta_{1\text{-}40}$. The ratio of $C_1(0)/C_2(0)$ in sample with glucose remains constant for the first week then starts to decrease after 168 hrs (Fig. 5c). The intensity $C_1(0)$ and $C_2(0)$ both decrease as the sample ages (Figs. 5a and b). The decrease observed

in the $C_1(0)$ value is mostly because the number of monomers is reduced due to aggregation. The decrease in $C_2(0)$, on the other hand, might be a result of Tyr having a constantly changing quantum yield due to glucose-meditated aggregation. Unlike in the free $A\beta_{1-40}$, the $C_1(t)/C_2(t)$ plot is not sensitive to the age of the sample especially during the first 96 hrs (Fig. 5c).

To summarise, steady state spectra measurements reveal a variety of complexes formed during $A\beta_{1-40}$ oligomerisation, which also appear in the presence of glucose but at a much faster rate. The decrease observed in the Tyr peak ($\lambda_{max}\approx304$ nm) when excited with 279 nm is most likely a result of the decrease in the concentration of $A\beta_{1-40}$ monomers over 384 hr. In contrast, the increase observed in peaks ($\lambda_{max}\approx330$-445 nm) excited with wavelengths $\geq$ 300 nm and their shift towards the red within 384 hr indicates the formation of aggregates which grow in number and size. The peak observed at 540 nm absorbs light between 279 and 320 nm and its location and intensity remain constant for both samples. We associate this peak with small complexes of $A\beta_{1-40}$. TRES measurements show that at excitation 279 nm, free $A\beta_{1-40}$ exhibits two forms of fluorescent species; monomers and a single type of aggregates that grows gradually and undergoes dielectric relaxation with rates that are basically controlled by the size of the aggregate. In the presence of glucose we believe that there is more than two fluorescent species: the typical monomers observed in free $A\beta_{1-40,}$ but at much lower concentrations, and more than one type of oligomers each with its own fluorescence intensity decay and dielectric relaxation rate. This demonstrates that glucose alters the aggregation pathway. These changes are highly relevant to our understanding of the pathophysiology of AD and the implication of AGE and diabetes in these pathways. Such an understanding and disease modelling may aid testing of interventions including pharmacotherapies that may ameliorate disease progression.

Experimental Methods

Sample preparation

Re-suspending the lyophilised peptide (Aβ1-40; Anaspec Inc, USA) was achieved by the treatment in 1,1,1,3,3,3- Hexafluoro-2-Propanol (HFIP; Sigma-Aldrich, UK). Aβ1-40 was diluted in 100% HFIP to 0.1 mM and sonicated for 10 minutes. The clear solution containing the dissolved peptide was then aliquoted in Eppendorf microcentrifuge tubes and the HFIP was allowed to evaporate in a fume hood. The samples were then stored at -20 °C.

For steady-state measurements the samples were diluted in 0.1 mM of 4-(2-hydroxyethyl)-1-piperazineethanesulfonic acid (HEPES; Sigma-Aldrich, UK) and a Phosphate-Buffered Saline PBS (PBS; Sigma-Aldrich, USA) solution with a phosphate buffer concentration of 0.01 M, 0.0027 M

potassium chloride and 0.137 M sodium chloride. No differences in beta-amyloid spectra were observed for different buffers. HEPES–based samples were used in lifetime measurements. The final concentration of Aβ1-40 was 50 μM and at pH 7.4. To study Aβ1-40 glycation, Glucose (D-(+)-glucose; (Sigma-Aldrich, USA) was added to the samples to a concentration of 50 mM. The amyloid suspensions were kept in a micro-cuvette with a volume of ∼140 μl and were not stirred during the experiment. The experiments were performed at 37°C and all components and solutions were in thermal equilibrium before use.

Steady-state measurements

Steady-state fluorescence spectral measurements of $A\beta_{1\text{-}40}$ were obtained using a Fluorolog-3 spectrofluorometer. The excitation and emission monochromators were set at 5-nm slit widths. Measurements were taken at Excitations 279, 290, 300, 320, 350 and 380 nm. Emission was monitored over a range of wavelengths in increments of 1 nm at different times: 1, 24, 168 and 384 hours after sample preparation (Supplementary Fig. 1).

Time-correlated single photon counting (TCSPC)

TCSPC measurements were conducted on a Horiba Scientific DeltaFlex fluorometer (HORIBA Jobin Yvon IBH Ltd,Glasgow,UK). The system was equipped with Seya-Namioka monochromators for excitation and emission. The excitation source used was a HORIBA NanoLED with a centre wavelength of 279 nm, pulse duration of 50 ps and a repetition rate of 1 MHz[33].

A series of 12 fluorescence decay curves were collected at the emission wavelengths between 294 and 327 nm at 3 nm increments. Supplementary Fig. 2 shows an example of three fluorescence decays measured at different stages of aggregation (1, 48 and 168 hrs) for free Aβ and Aβ with glucose.

Fluorescence decay curves were analysed by two alternative deconvolution programs. Both capable of coping with the expected scattered light but by different approaches. The first, DAS6 - the commercial HORIBA Scientific software, represents the scattered light as an additional component with a fixed short lifetime in the *(n+1)*-exponential model decay function (Supplementary Fig. 3).

The second deconvolution software assumes *n*-exponential decay of fluorescence intensity and directly accounts for the presence of scattered excitation light in the Tyr decay (Supplementary Fig. 4)

$$F(t) = a + bL(t + \Delta) + c\int_0^t L(t + \Delta - t')I(t')dt' \qquad (2)$$

where *L(t)* is the prompt excitation function, *a*, *b*, and *c* are the background level, contribution of the scattered light and the scaling parameter, respectively, and Δ is the time-shift between the prompt and decay curves due to the colour effect of the light detector. *I(t)* is the *n*-exponential model function. This approach was applied to obtain the parameters of the decays used in TRES analysis.

Calculating time resolved emission spectra (TRES)

The reason why we decided to use the TRES approach, instead of applying the fluorescence intensity decay analysis based on measurements at a single wavelength, was expected complexity of the fluorescence kinetics of $A\beta_{1\text{-}40}$, where the decay of the population of excited molecules is disturbed by the shifts in the transient emission spectra. TRES approach allows resolving these processes. The fluorescence decays $I_\lambda(t)$, measured at individual wavelengths λ were fitted to multi-exponential functions and then used to calculate the TRES $I_t(\lambda)$ from the equation

$$I_t(\lambda) = I_\lambda(t) \times \frac{S(\lambda)}{\int_0^\infty I_\lambda(t)dt} \qquad (3)$$

where $S(\lambda)$ is the steady-state fluorescence spectrum, and the integral is proportional to the total emitted photons in the lifetime experiment. The obtained spectra were then converted from the wavelength $I_t(\lambda)$ to the wavenumber scale according to $I_t(\nu) = \lambda^2 I_t(\lambda)$.

TRES were obtained for $A\beta_{1\text{-}40}$ at several stages of aggregation, namely 1, 5, 24, 48, 72, 96 and 168 hrs after sample preparation (the number indicates the age of the sample when the measurement at the first wavelength has been started). From the data obtained for each stage of aggregation, 14 TRES were calculated at different times after excitation. Supplementary Fig. 5 shows the TRES of samples in the absence and presence of 50 mM of glucose at different stages of aggregation (i.e. 1, 24, 48, 72, 96 and 168 hours)

According to Toptygin and Brand[32] the fluorescence spectrum of a single fluorescent residue can be expressed as $\sim \nu^3 g(\nu)$, where $g(\nu)$ is the Gaussian distribution function. Therefore, for the purpose of detailed analysis of the $A\beta_{1\text{-}40}$ TRES we modelled the recovered spectra $I_t(\nu)$ at the time t as the sum of N components of the type $\sim \nu^3 g(\nu)$ as described in equation (1)

The obtained experimental TRES for the sample with and without glucose demonstrate the presence of two components (N=2). The parameters recovered from fitting the proposed model (equation (1) for N=2) to the experimental data were used to analyse and compare the fluorescence kinetics of both samples.

Associated Context

The Supporting Information (SI) is available free of charge on the ACS Publications website at DOI:

Author Information

*E-mail: o.j.rolinski@strath.ac.uk

Acknowledgements

A. Alghamdi wishes to thank PNU for financial support.

References

1. Bush, A. I. The metallobiology of Alzheimer's disease. *Trends Neurosci.* ***2003****, 26, 207–214.*

2. Adlard, P. A. & Bush, A. I. Metals and Alzheimer's disease. *J. Alzheimer's Dis.* ***2006****, 10, 145–163.*

3. Vitek, M. P. *et al.* Advanced glycation end products contribute to amyloidosis in Alzheimer disease. *Proc. Natl. Acad. Sci.* ***1994****, 91, 4766–4770.*

4. Münch, G. *et al.* Influence of advanced glycation end-products and AGE-inhibitors on nucleation-dependent polymerization of β-amyloid peptide. *Biochim. Biophys. Acta (BBA)-Molecular Basis Dis.* ***1997****, 1360, 17–29.*

5. Srikanth, V. *et al.* Advanced glycation endproducts and their receptor RAGE in Alzheimer's disease. *Neurobiol. Aging.* ***2011****, 32, 763–777.*

6. Coker, L. H. & Wagenknecht, L. E. Advanced glycation end products, diabetes, and the brain. *Neurology* ***2011****, 77(14), 1326-1327.*

7. Smith, M. A., Vitek, M. P., Monnier, V. M. & Perry, G. Early AGEing and Alzheimer's. *Nature* ***1995****, 374, 316.*

8. Yaffe, K. *et al.* Advanced glycation end product level, diabetes, and accelerated cognitive aging. *Neurology* ***2011****, 77, 1351–1356.*

9. Sasaki, N. *et al.* Advanced glycation end products in Alzheimer's disease and other neurodegenerative diseases. *Am. J. Pathol.* ***1998****, 153, 1149–1155.*

10. Takeuchi, M. & Yamagishi, S. Possible involvement of advanced glycation end-products (AGEs) in the pathogenesis of Alzheimer's disease. *Curr. Pharm. Des.* ***2008****, 14, 973–978.*

11. Li, X. H. *et al.* Glycation exacerbates the neuronal toxicity of β-amyloid. *Cell Death Dis.* ***2013****, 4, e673.*

12. Chen, C. *et al.* Aβ-AGE aggravates cognitive deficit in rats via RAGE pathway. *Neuroscience* ***2014****, 257, 1–10.*

13. Chaney, M. O. *et al.* RAGE and amyloid beta interactions: atomic force microscopy and molecular modeling. *Biochim. Biophys. Acta (BBA)-Molecular Basis Dis.* ***2005****, 1741, 199–205.*

14. Chen, K., Kazachkov, M. & Yu, P. H. Effect of aldehydes derived from oxidative deamination and oxidative stress on β-amyloid aggregation; pathological implications to Alzheimer's disease. *J. Neural Transm.* ***2007****, 114, 835–839.*

15. Chen, K., Maley, J. & Yu, P. H. Potential implications of endogenous aldehydes in β-amyloid misfolding, oligomerization and fibrillogenesis. *J. Neurochem.* ***2006****, 99, 1413–1424.*

16. Pike, C. J., Overman, M. J. & Cotman, C. W. Amino-terminal deletions enhance aggregation of β-amyloid peptides in vitro. *J. Biol. Chem.* ***1995****, 270, 23895–23898.*

17. LeVine III, H. [18] Quantification of β-sheet amyloid fibril structures with thioflavin T. *Methods in enzymology* ***1999****, 309, 274–284.*

18. Luchsinger, J. A., Tang, M.-X., Stern, Y., Shea, S. & Mayeux, R. Diabetes mellitus and risk of Alzheimer's disease and dementia with stroke in a multiethnic cohort. *Am. J. Epidemiol.* ***2001****, 154, 635–641.*

19. Lee, J., Culyba, E. K., Powers, E. T. & Kelly, J. W. Amyloid-β forms fibrils by nucleated conformational conversion of oligomers. *Nat. Chem. Biol.* ***2011****, 7, 602.*

20. Ono, K. & Yamada, M. Low-n oligomers as therapeutic targets of Alzheimer's disease. *J. Neurochem.* ***2011****, 117, 19–28*.

21. Gadad, B. S., Britton, G. B. & Rao, K. S. Targeting oligomers in neurodegenerative disorders: lessons from α-synuclein, tau, and amyloid-β peptide. *J. Alzheimer's Dis.* ***2011****, 24, 223–232* .

22. Amaro, M., Birch, D. J. S. & Rolinski, O. J. Beta-amyloid oligomerisation monitored by intrinsic tyrosine fluorescence. *Phys. Chem. Chem. Phys.* ***2011,*** *13, 6434–6441*.

23. Wu, J. W. *et al.* Fibrillar oligomers nucleate the oligomerization of monomeric amyloid β but do not seed fibril formation. *J. Biol. Chem.* ***2010****, 285, 6071–6079*.

24. Chen, W.-T., Liao, Y.-H., Yu, H.-M., Cheng, I. H. & Chen, Y.-R. Distinct effects of Zn2+, Cu2+, Fe3+, and Al3+ on amyloid-β stability, oligomerization, and aggregation: amyloid-β destabilization promotes annular protofibril formation. *J. Biol. Chem.* ***2011****, 286, 9646–9656*.

25. Sengupta, U., Nilson, A. N. & Kayed, R. The role of amyloid-β oligomers in toxicity, propagation, and immunotherapy. *EBioMedicine* ***2016****, 6, 42–49.*

26. Younan, N. D. & Viles, J. H. A comparison of three fluorophores for the detection of amyloid fibers and prefibrillar oligomeric assemblies. ThT (thioflavin T); ANS (1-anilinonaphthalene-8-sulfonic acid); and bisANS (4, 4′-dianilino-1, 1′-binaphthyl-5, 5′-disulfonic acid). *Biochemistry* ***2015****, 54, 4297–4306.*

27. D'Amico, M. *et al.* Thioflavin T promotes Aβ (1–40) amyloid fibrils formation. *J. Phys. Chem. Lett.* ***2012****, 3, 1596–1601*.

28. Amaro, M., Wellbrock, T., Birch, D. J. S. & Rolinski, O. J. Inhibition of beta-amyloid aggregation by fluorescent dye labels. *Appl. Phys. Lett.* ***2014****, 104(6), art. No. 063704*.

29. Rolinski, O. J., Amaro, M. & Birch, D. J. S. Biosensors and Bioelectronics Early detection of amyloid aggregation using intrinsic fluorescence. *Biosens. Bioelectron.* ***2010****, 25, 2249–2252*.

30. Rolinski, O. J., Wellbrock, T., Birch, D. J. S. & Vyshemirsky, V. Tyrosine photophysics during the early stages of β-amyloid aggregation leading to Alzheimer's. *J. Phys. Chem. Lett.* ***2015****, 6, 3116–3120*.

31. Alghamdi, A., Vyshemirsky, V., Birch, D. J. S. & Rolinski, O. J. Detecting beta-amyloid aggregation from time-resolved emission spectra. *Methods Appl. Fluoresc.* ***2018****, 6, 024002*.

32. Toptygin, D. & Brand, L. Spectrally-and time-resolved fluorescence emission of indole during solvent relaxation: a quantitative model. *Chem. Phys. Lett.* ***2000****, 322, 496–502.*

33. Mcguinness, C. D., Sagoo, K., Mcloskey, D. & Birch, D. J. S. A new sub-nanosecond LED at 280 nm. *Meas. Sci. Technol.* ***2004****, 15, L19-22.*